Regular Article - Plasma Physics

QED effects at grazing incidence on solid-state targets

Marko Filipovic[a] and Alexander Pukhov[b]

Institut für Theoretische Physik I, Heinrich-Heine-Universität Düsseldorf, Universitätsstraße 1, 40225 Düsseldorf, Germany

Abstract. New laser facilities will reach intensities of 10^{23} W cm^{-2}. This advance enables novel experimental setups in the study of laser–plasma interaction. In these setups with extreme fields, quantum electrodynamic (QED) effects such as photon emission via nonlinear Compton scattering and Breit–Wheeler pair production become important. We study high-intensity lasers grazing the surface of a solid-state target by two-dimensional particle-in-cell simulations with QED effects included. The two laser beams collide at the target surface at a grazing angle. Due to the fields near the target surface, electrons are extracted and accelerated. Finally, the extracted electrons collide with the counter-propagating laser, which triggers many QED effects and leads to a QED cascade under a sufficient laser intensity. Here, the processes are studied for various laser intensities and angle of incidence and finally compared with a seeded vacuum cascade. Our results show that the proposed target can yield many orders of magnitude more secondary particles and develop a QED cascade at lower laser intensities than the seeded vacuum alone.

1 Introduction

With the construction of high-intensity laser facilities such as ELI [2], XCELS [3], SEL [4], SULF [5] and Apollon [6], the study of laser–matter interaction in strong electromagnetic fields has been greatly advanced. The development of these lasers is possible due to the chirped pulse amplification [7] which revolutionized the high-intensity laser technology. One of the natural applications for such lasers is the high-energy electron acceleration that can in turn be used to study fundamental quantum physics [8–10].

Two of the QED effects that can take place when relativistic electrons interact with a strong electromagnetic field are the emission of hard photons by nonlinear Compton scattering and electron–positron pair production with the multi-photon Breit–Wheeler process [11–13]. In order to quantify whether the mentioned interactions take place, the quantum nonlinearity parameter χ has been defined and reads

$$\chi = \sqrt{-\left(F_{\mu\nu}p^{(\nu)}\right)^2}/(m_e c E_{cr}) \tag{1}$$

or simplified

$$\chi = \frac{e\hbar}{m^2 c^3}\sqrt{\left(\gamma\mathbf{E} + \frac{\mathbf{p}}{mc}\times\mathbf{B}\right)^2 - \left(\frac{\mathbf{p}}{mc}\cdot\mathbf{E}\right)^2} \tag{2}$$

where E_{cr} is the critical field of vacuum breakdown also known as the Schwinger limit [14]; $F_{\mu\nu}$ the electromagnetic field tensor; and $p^{(\nu)}$ the four-dimensional momentum. The quantum parameter χ defines whether the processes are treated in classical electrodynamics or quantum electrodynamics and is often used in computational tools to calculate probabilities for QED effects [15]. Once $\chi \geq 1$, the radiation processes should be treated in quantum electrodynamics [16]. This has been also experimentally observed, where radiation reaction was the subject of study and a sole classical description was insufficient to fully understand the radiation process [17,18].

Photon emission and pair production may continue repetitively in a strong electromagnetic field and lead to QED cascades [15,19–24,39]. This may result in an electron–positron plasma of high density. Electrons and positrons oscillating in the strong electromagnetic fields emit photons, while the new photons decay again to an electron–positron plasma, which have the possibility again to repeat the cycle.

The χ-parameter also classifies different QED regions besides distinguishing how to treat processes. The supercritical regime corresponds to a limit of $\chi \gg 1$ [25], and after reaching $\alpha\chi^{2/3} \geq 1$, it is conjectured that QED theory becomes nonperturbative [26,27]. Here, α denotes the fine structure constant. The fully nonperturbative QED (FNQED) regime is still not experimentally explored, but various initial analytic studies were conducted [28–30].

[a] e-mail: marko.filipovic@hhu.de (corresponding author)
[b] e-mail: pukhov@tp1.uni-duesseldorf.de

A second important parameter for QED studies which describes whether a field is able to accelerate an electron to relativistic energies is

$$a_0 = \frac{|e|E_L}{m_e c \omega_0} \tag{3}$$

the dimensionless field amplitude [11] with ω_0 the laser frequency. Previously mentioned lasers facilities will be able to provide the necessary parameter of $a_0 \gg 1$ to witness relativistic particles and observe QED effects within promising configurations if the quantum parameter χ is big enough. Such configurations have been proposed by using lasers with near-critical plasma [8–10,31] or thin foils [32].

The challenge to reach the new QED regimes is to generate strong fields and high-energetic particles at the same time. These allow particles to achieve a high quantum parameter. Possible setups to study new QED regimes are the collision between an electron beam and a laser pulse with an intensity of $10^{24} \mathrm{Wcm}^{-2}$ [33], collision of high-current 100GeV electron bunches [34], collision of an ultra-relativistic electron beam with a counter-propagating ultraintense electromagnetic pulse [35] and other configurations [36–38].

Numerical particle-in-cell (PIC) simulations which research particle dynamics of laser–plasma interactions are an important tool to study QED effects [40–42]. These codes can include QED effects to simulate future experiments. Here, we use the PIC code VLPL [43] with the QED module [15,44] to study the proposed configuration in regard to nonlinear Compton scattering and multi-photon Breit–Wheeler pair production.

The work in this paper focuses on the effect of high-intensity lasers at grazing incidence to study QED effects and QED cascades on a solid density target. The PIC code not only simulates charged particles (electrons, positrons, ions), but also treats γ-photons as numerical particles. This allows us to generate γ-photons by initializing a laser that propagates towards a solid-state target to extract and accelerate electrons and emit photons by the nonlinear Compton scattering. Therefore, the proposed configuration uses two high-intensity lasers that collide on the surface of the target. Using a small grazing incidence achieves a higher Lorentz factor for the extracted particles and a greater current of the extracted electron bunch [45].

In the work of Grismayer et al. [22], QED cascades were studied, and it was determined that configurations with maximal pair growth are desired. For this reason, setups that provide the highest values of the quantum parameter are likely to produce a cascade. The quantum parameter as described in Eq. 2 increases with greater γ-values. Taking a look now at laser beams at grazing incidence, which we use here, the work of Serebryakov et al. [45] estimates $\gamma_{\max}$ at an angle of incidence Θ with

$$\gamma_{\max}(\Theta) \approx 1 + \frac{4a_0 \sin \Theta}{1 - \cos \Theta}. \tag{4}$$

Lowering Θ gains us a higher γ-value. An estimation with Eq. 4 gives a $\gamma_{\max}$ of $\sim$ 12,150 for $\Theta = 15°$ and $a_0 = 400$ if the particle remains in the maximum number of field periods, where it can be accelerated [45]. These electrons can benefit cascading if we take a look now at the probability rates of photon emission and pair production process, the two dominant processes.

Simple asymptotic expression in the limit of large χ_e for electrons and χ_γ was provided in [15] and read

$$W_{\mathrm{rad}} \approx 1.46 \frac{\alpha m^2 c^4}{\hbar \varepsilon_e} \chi_e^{2/3} \tag{5}$$

and

$$W_{\mathrm{pairs}} \approx 0.38 \frac{\alpha m^2 c^4}{\hbar \varepsilon_\gamma} \chi_\gamma^{2/3} \tag{6}$$

with W_{rad} the probability rate for photon emission, W_{pair} the probability rate for pair creation by hard photons and ε the energy of the appropriate particle. Here, we can see electrons with a high χ are more likely to emit photons and high-energy γ-photons decay easier to electron–positron pairs since the probabilities increase with higher χ. In the proposed configuration, the second counter-propagating laser beam, respectively, for both sides, supplies a strong electromagnetic field to increase the χ-parameter again. Therefore, QED processes are very likely and repeat, which leads to cascading.

The paper is organized as follows. In Sect. 2, we describe the simulation configuration with the parameters of the domain, target and laser beams. A brief summary of the used QED module will be given as well. Section 3 presents the results of particle-in-cell simulations and the generation of electron–positron plasma in this configuration. We compare the electron–positron plasma production near a solid density surface with the vacuum case. Section 4 summarizes the main results of our study and gives a prospect to the future of this subject.

2 Simulation setup

The particle-in-cell (PIC) simulations are performed in a two-dimensional (2D) geometry using the Virtual Laser Plasma Lab (VLPL) code [40,43]. The simulation domain is $100\lambda_0$ and $50\lambda_0$ in x- and y-direction ($\lambda_0 = 910\mathrm{nm}$ is the laser wavelength) with a spatial grid step of $0.02\lambda_0 \times 0.05\lambda_0$, respectively. The electromagnetic fields are updated with the X-dispersionless Maxwell solver [46], also known as RIP solver. The Maxwell solver requires $h_x = c\tau = 0.02\lambda_0$ with h_x the longitudinal grid step and τ the time step. A simulation runs for $120T_0$ with $T_0 \approx 3.04\mathrm{fs}$ being the laser period. The basic configuration is shown in Fig. 1. The
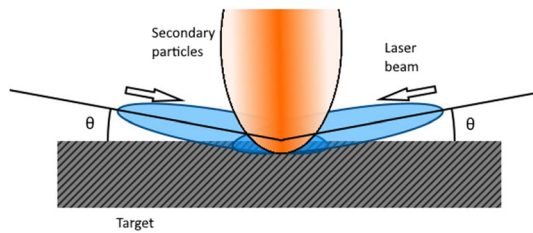
Fig. 1 Configuration of two high-intensity lasers grazing a solid-state target. Arrows indicates the trajectory of each laser beam. The lasers are focused on the centre of the upper edge of the target. Both lasers are incident on the same angle Θ. The orange half ellipsis shows the region where secondary particles from QED effects will be located after the interaction

solid-state target is located in the lower half of the simulation domain. The electron density is $505.55n_{cr}$. Here, $n_{cr} \sim 1.35 \times 10^{21} \text{cm}^{-3}$ is the critical density for the considered wavelength λ_0. Absorbing boundary conditions were chosen for the domain. The electrons are represented by four particles per cell.

Both lasers are linearly p-polarized Gaussian beams with $a = a_0 \exp\left(-(x - ct)^2/\tau^2 - y^2/\sigma_y^2\right)$ with $\tau = 8.240T_0$ and $\sigma_y = 5.978\lambda_0$. Each laser has a diameter of $5.978\lambda_0$ and a length of $8.240\lambda_0$. The two lasers are grazing the target at different grazing angles $2.5° \geq \Theta \geq 15°$ ($1/72\pi \geq \Theta \geq 1/12\pi$) and are initialized $75\lambda_0$ away from their point of incidence. Point of incidence of both laser propagation axes is at the centre of the upper edge of the target. QED effects in `VLPL` are computed using the Monte Carlo method [15,44]. Evaluated in the simulation data are the nonlinear Compton scattering and the Breit–Wheeler process. Collisions are neglected in the simulations.

Photon emission and the pair production have been implemented in QED sub-routines. Both routines are using the Monte Carlo approach and utilize the alternate model by Elkina et al. [15]. The first sub-routine which is called in a PIC loop is computing the Breit–Wheeler pair production that is run before updating the momentum of the particles in case the photon decays and does not require further calculations. First, a random number $r_1\epsilon[0,1]$ is decided which represents the possible energy of the electron of the pair. Afterwards, the probability rate is calculated with

$$\frac{dW_{\text{pair}}}{d\varepsilon_e} = \frac{\alpha m^2 c^4}{\hbar\varepsilon_\gamma^2} \left[\int_x^\infty \text{Ai}(\xi)\, d\xi + \left(\frac{2}{x} - \chi_\gamma\sqrt{x}\right)\text{Ai}'(\chi) \right]. \quad (7)$$

A second random number decides whether the process occurs. The condition that needs to be fulfilled is

$$r_2 < [dW_{\text{pair}}/d\varepsilon_e]\,\varepsilon_\gamma\tau. \quad (8)$$

If the algorithm succeeds, the photon gets deleted and electron and positron macro-particles are imple-

mented in the simulation domain at the same place. The momentum of the pair abides the conservation of momentum. In the same manner, the photon emission is simulated after the momentum update with its corresponding probability rates. Here, a photon is placed at the same location as the emitting particle and both particle momenta are calculated by the conservation of momentum.

3 Results

The first simulation presented uses lasers with an incident angle of $\Theta = 15°$ and an $a_0 = 1200$. After the initialization, the lasers propagate along the surface extracting, capturing and accelerating electrons in the electromagnetic fields of the lasers (Fig. 2 first row). These electrons co-move with the laser along the surface (Fig. 2 second row $t = 55T_0$). In the process, the particles of the target emit photons, which is shown in Fig. 2 (fourth row). The energy density of the emitted photons is similarly structured to the propagating electromagnetic waves since the probability rate of the process is tied to the χ-parameter, which includes the electromagnetic fields.

The trapped electrons and emitted photons produced by one laser beam collide with the counter-propagating laser beam and particles. In the interaction region, where both laser beams overlap, the nonlinear Breit–Wheeler pair production becomes likely. At this point, the χ-parameter rises to a value of 9.65 due to the strong field that a particle comes in contact within its rest frame. Photons decay in an electron–positron pair, which is represented in Fig. 2 (third row) during the overlap (middle column) at $t = 75T_0$. An electron–positron plasma builds up in the region and expands outwards in the positive y-direction, where the target is not obstructing fields and particle dynamics, while reaching a higher peak density than the initial solid-state target. Pair production processes started to be recorded once the counter-propagating beam reaches the centre, since the fields near the surface are not sufficient to trigger the effect with the co-moving photons. In addition to the emitted photons by grazing the target, the collision of the extracted electrons and the respective laser triggers photon emission again, which fuels the electron–positron plasma. Once the field is partially absorbed by the electron–positron plasma, the new plasma is shielded by the remaining electromagnetic field (Fig. 2 first row) at $t = 85T_0$. Several cycles of the emission of hard photons and the conversion of electron–positron pairs are observed leading to the electron–positron plasma by this QED cascade.

Figure 3 shows the spectra of electrons, positrons and γ-photons at four different time instances. The first displayed time at $t = 55T_0$ shows the energy spectrum after extracting and accelerating some electrons by the incident laser beams. Electrons, represented in subplot (a), are accelerated up to 3GeV. Pair production at the early stage without interacting with the counter-
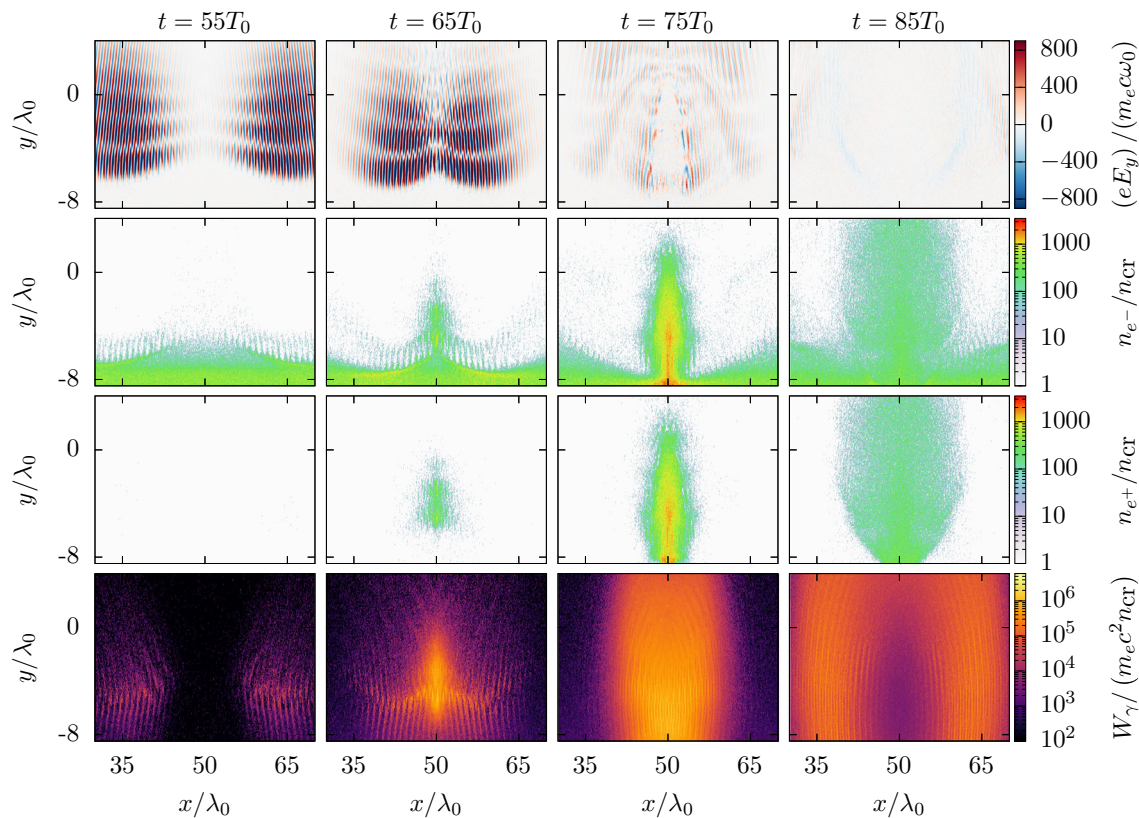
Fig. 2 E_y-component in dimensionless units (first row), electron density distribution in critical densities (second row), positron density in critical densities (third row) and energy density of emitted photons (fourth row) at different time instances in QED-PIC simulation with parameters $a_0 = 1200$ and $\theta = 15°$

propagating electromagnetic field (see subplot c) occurs only in a low number. Here, it can be seen that the positron spectrum at $t = 55T_0$ only shows some noise in the low-energy region by a low number of pair production processes. This observation is in agreement with the rise of the electron–positron plasma shown in Fig. 2.

Continuing with the photon emission, γ-photons are emitted at two points in the configuration. First, photon emission takes place once the laser beam comes into contact with the target and then continuously emits photons while scraping the surface, which can be seen in the energy densities of Fig. 2 (fourth row). The corresponding spectra to the displayed energy densities are shown in Fig. 3b. At $t = 55T_0$, the continuous photon spectrum contains mainly low-energy photons. Second, the accelerated and extracted electrons collide with the counter-propagating beam and radiate high-energy photons due to the stronger electromagnetic field perceived in the electrons rest frame. The photon spectrum at $t = 65T_0$ gains, in comparison with the previous time, photons across the whole recorded energy range, as the front of the counter-propagating laser reaches the point, where the propagation axes of both laser beams intersect at the surface (Fig. 2 at $t = 65T_0$). In the time instance $t = 75T_0$ and forward the number of photons increases by several orders of magnitudes. The radia-

tion reaction is now significantly stronger, leading to the great yield of emitted γ-photons. Additionally, the maximum energy of the γ-photons slightly decreases between the times $t = 65T_0$ and $t = 75T_0$. The reason for this change is the high probability of high-energy photons undergoing the pair production process.

As the electron beam interacts with the counter-propagating laser beam the number of positrons increases (Fig.3c). This indicates that the probability for pair production processes became more likely and the process is triggered. Both the electron and positron spectrum roughly coincide. With both laser beams starting to overlap, the maximum recorded electron and positron energy drops to ~ 1GeV by $t = 75T_0$. The electrons and positrons lose their energy due to the radiation reaction with the laser beams. It can be observed as the increase of low-energy electrons and positrons in their respective spectrum. At the same time, more γ-photons are emitted that further produce electron–positron pairs. This is shown by the positron spectrum in subplot (c) at $t = 75T_0$.

In a next step, the influence of the laser parameters will be discussed. Figure 4 shows the photon spectrum and positron spectrum for different laser amplitudes ranging from 400 to 2000. In general, increasing the energy of the laser beam boosts the secondary particle spectra. Additionally, the cutoff energy of the
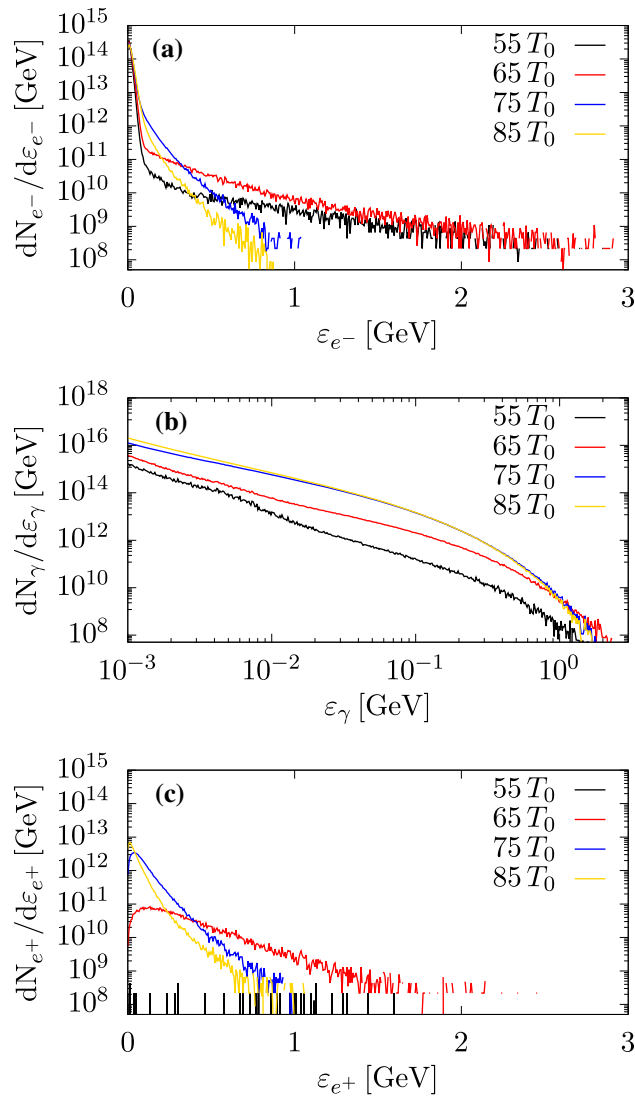
Fig. 3 Particle spectrum of electrons (**a**), photons (**b**) and positrons (**c**) at $t = 55T_0, 65T_0, 75T_0$ and $85T_0$, respectively. The highest peak of the laser beam reaches the centre of the surface at $t = 75T_0$. Laser parameters are $a_0 = 1200$, and angle of incidence is $\Theta = 15°$
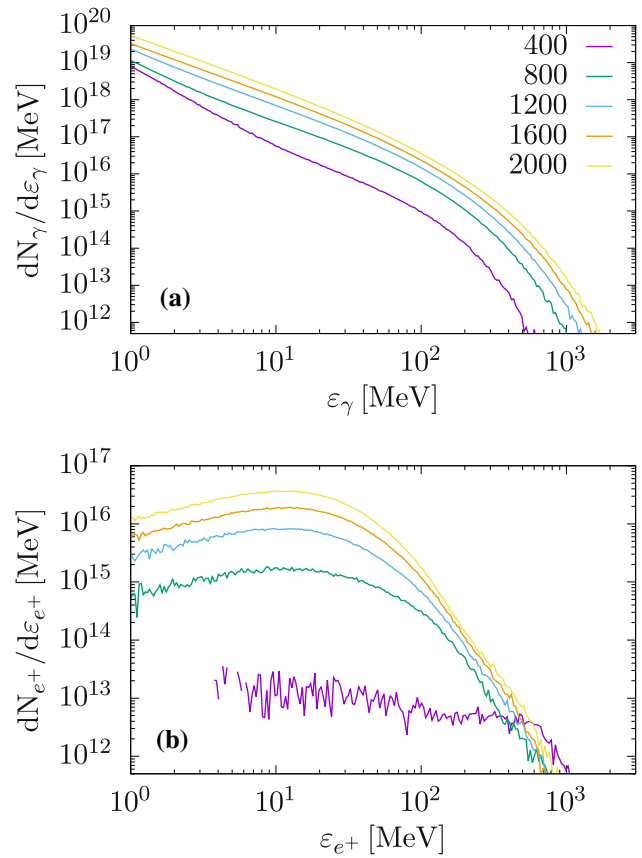

Fig. 4 Double logarithmic spectrum of emitted photons (**a**), and logarithmic spectrum of positrons (**b**) after the overlap of the high-intensity lasers for different a_0 pulses. Angle of incidence for both configurations is $\Theta = 15°$
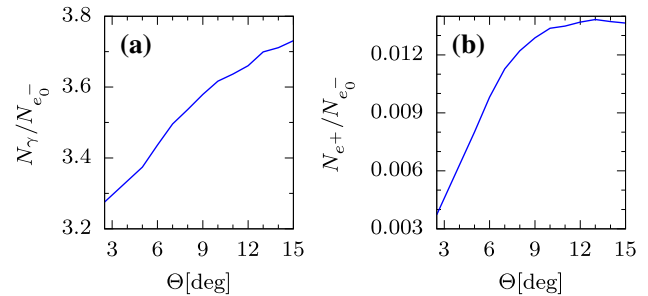

Fig. 5 Ratio of emitted photons to the initial number of electrons (**a**), ratio of electron–positron pairs to the initial number of electrons (**b**). a_0 is set to 800

photon drifts to a higher value by increasing a_0. In the special case of $a_0 = 400$, the characteristic spectrum of positrons is not reproduced since the statistic is insufficient and the electromagnetic fields are not strong enough to develop the positron spectrum. Only by reaching an $a_0 \sim 800$, pair processes are sufficiently witnessed and an electron–positron plasma builds up.

The other laser parameter in the proposed configuration is the angle of incidence Θ. In a second simulation series, the angle has been varied between 2.5 and 15 [deg] while maintaining the dimensionless vector amplitude at $a_0 = 800$. Figure 5 shows the ratios for emitted photons (subplot a) and positrons (subplot b) per initial electron. In general, fractions of secondary particles increase with a larger angle Θ. Further, positrons of the pair production per initial electrons are maximized at an angle of $\sim 10°$, whereas photons remain to

increase with bigger angles. A possibility for this observation may be the energy loss of the electromagnetic fields. The fields are absorbed by the electron–positron plasma in the interaction region. When the laser energy is depleted, the pair production ceases and the ratio of positrons per initial electrons is maximized. While this is the case for pair production, photons may still be emitted with a weaker field. Fraction of photons per initial electron continue to rise after an incident angle of $10°$.

The previous results showed that QED effects were observed in the proposed configuration. In a final step,
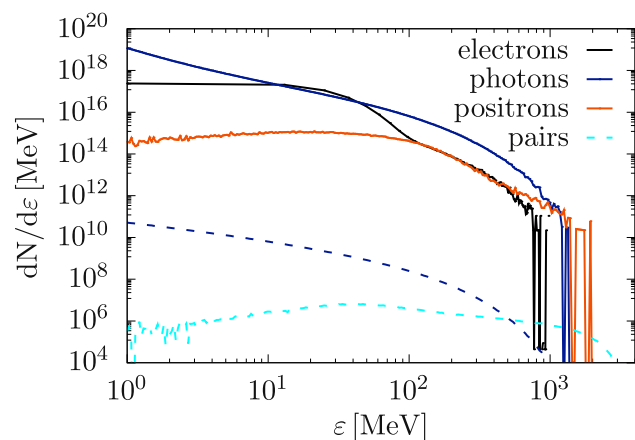
Fig. 6 Double logarithmic spectrum of secondary particles. Solid line represents the configuration of grazing a solid-state target; dashed line is the seeded vacuum configuration. Spectrum after the overlap of the high-intensity lasers at $t = 90T_0$. Angle of incidence for both configuration is $\Theta = 12°$ and $a_0 = 800$. Additionally, the cyan line represents the electron and positron spectrum, since both spectra are equal due to the small number of seed electrons

the configuration will be compared to a seeded vacuum cascade [19,47,48]. Setting up a configuration for a vacuum cascade appears to be simpler; therefore, it is reasonable to compare both configurations. A seeded vacuum may resemble an imperfect vacuum, where a small impurity remains after trying to create a vacuum. Seed electrons are necessary to initiate QED effects in the code. Figure 6 shows a comparison between the proposed configuration and the seeded vacuum within the secondary particle spectra for lasers with $a_0 = 800$ and $\theta = 12°$. 72 seed electrons are initialized in two cells where the propagation axes of the lasers intersect. The electron density in those cells is $7.39 \times 10^{-7} n_{cr}$. Here, the solid-state target emits many order of magnitudes of photons more than the seeded vacuum cascade. While emitting less photons, the vacuum cascade manages to accelerate the positrons created by pair production process to an energy of $\sim 3\text{GeV}$ seen in the increased cutoff energy. The proposed configuration still outperforms the vacuum scenario in the yield of pairs. However, the maximum photon energy achieved is $\sim 1400\text{MeV}$.

4 Conclusion

In this paper, the interaction of two high-intensity lasers and a solid-state target was studied in the framework of PIC simulations. Focus was placed on QED processes where both lasers overlap and interact with extracted and accelerated electrons. The large number of the extracted electrons escalates into a QED cascade creating an electron–positron plasma once the laser intensity was sufficiently high. Comparing the plasma with a seeded vacuum cascade demonstrated that using a target outperforms an imperfect vacuum.

Further, increasing the angle of incidence reached an upper limit on produced pairs by QED effects on the electron–positron plasma and higher lasers intensities showed that a certain laser intensity is necessary to trigger pair production processes.

Additional studies should be performed on different potential target materials and other forms to enhance the achieved quantum parameter or increase the number of QED processes.

In the near future where higher intensities are reached, this configuration may be replicated experimentally and help to achieve even not yet experimentally explored regimes like the fully nonperturbative regime.

Author contributions

AP conceived the configuration, and MF carried out all simulations and performed data analysis. MF and AP clarified details of the physics and contributed to the writing of the manuscript. The first draft of the manuscript was written by MF, and all authors commented on it.

Data Availability Statement This manuscript has no associated data or the data will not be deposited. [Authors' comment: The data sets generated during and/or analysed during the current study are available from the corresponding author on reasonable request.

Declarations

Conflict of interest The authors declare that they have no conflict of interest.

Code availability The PIC code VLPL is available from A.P. on reasonable request.

References

1. Jülich Supercomputing Centre, JUWELS Cluster and Booster: Exascale Pathfinder with Modular Supercomputing Architecture at Juelich Supercomputing Centre. J. Large-Scale Res. Facilit. **7**(A138) (2021). https://doi.org/10.17815/jlsrf-7-183

2. *Whitebook ELI - Extreme Light Infrastructure: Science and Technology with Ultra-Intense Lasers* (2011). https://eli-laser.eu/media/1019/eli-whitebook.pdf

3. Whitebook XCELS - Exawatt Center for Extreme Light Studies (2009). https://xcels.ipfran.ru/img/XCELS-Project-english-version.pdf

4. X. Wang, X. Liu, X. Lu, J. Chen, Y. Long, W. Li, H. Chen, X. Chen, P. Bai, Y. Li, Y. Peng, Y. Liu, F. Wu, C. Wang, Z. Li, Y. Xu, X. Liang, Y. Leng, R. Li, 13.4 fs, 0.1 hz opcpa front end for the 100 pw-class laser facility. Ultrafast Science 2022, 9894358 (2022). https://doi.org/10.34133/2022/9894358

5. W. Li, Z. Gan, L. Yu, C. Wang, Y. Liu, Z. Guo, L. Xu, M. Xu, Y. Hang, Y. Xu et al., 339 j high-energy ti: sapphire chirped-pulse amplifier for 10 pw laser facility. Opt. Lett. **43**(22), 5681–5684 (2018). https://doi.org/10.1364/OL.43.005681

6. C.N. Danson, C. Haefner, J. Bromage, T. Butcher, J.C.F. Chanteloup, E.A. Chowdhury, A. Galvanauskas, L.A. Gizzi, J. Hein, D.I. Hillier et al., Petawatt and exawatt class lasers worldwide. High Power Laser Sci. Eng. **7**, e54 (2019). https://doi.org/10.1017/hpl.2019.36

7. D. Strickland, G. Mourou, Compression of amplified chirped optical pulses. Opt. Commun. **55**(6), 447–449 (1985). https://doi.org/10.1016/0030-4018(85)90151-8

8. J. Zhao, Y.T. Hu, Y. Lu, H. Zhang, L.X. Hu, X.L. Zhu, Z.M. Sheng, I.C.E. Turcu, A. Pukhov, F.Q. Shao, T.P. Yu, All-optical quasi-monoenergetic gev positron bunch generation by twisted laser fields. Commun. Phys. **5**(1), 15 (2022). https://doi.org/10.1038/s42005-021-00797-9

9. I.C.E. Turcu, B. Shen, D. Neely, G. Sarri, K.A. Tanaka, P. McKenna, S.P.D. Mangles, T.P. Yu, W. Luo, X.L. Zhu et al., Quantum electrodynamics experiments with colliding petawatt laser pulses. High Power Laser Sci. Eng. **7**, e10 (2019). https://doi.org/10.1017/hpl.2018.66

10. X.L. Zhu, T.P. Yu, M. Chen, S.M. Weng, Z.M. Sheng, Generation of gev positron and γ-photon beams with controllable angular momentum by intense lasers. New J. Phys. **20**(8), 083,013 (2018). https://doi.org/10.1088/1367-2630/aad71a

11. A.D. Piazza, C. Müller, K.Z. Hatsagortsyan, C.H. Keitel, Extremely high-intensity laser interactions with fundamental quantum systems. Rev. Mod. Phys. **84**, 1177 (2012). https://doi.org/10.1103/RevModPhys.84.1177

12. N.B. Narozhny, A.M. Fedotov, Quantum-electrodynamic cascades in intense laser fields. Phys-Usp **58**(1), 95 (2015). https://doi.org/10.3367/ufne.0185.201501i.0103

13. A. Fedotov, A. Ilderton, F. Karbstein, B. King, D. Seipt, H. Taya, G. Torgrimsson. Advances in qed with intense background fields (2022). https://doi.org/10.48550/ARXIV.2203.00019. https://arxiv.org/abs/2203.00019

14. J. Schwinger, On gauge invariance and vacuum polarization. Phys. Rev. **82**(5), 664 (1951). https://doi.org/10.1103/physrev.82.664

15. N.V. Elkina, A.M. Fedotov, I.Y. Kostyukov, M.V. Legkov, N.B. Narozhny, E.N. Nerush, H. Ruhl, QED cascades induced by circularly polarized laser fields. Phys. Rev. Spec. Top.: Accelerator Beams **14**(5), 054,401 (2011). https://doi.org/10.1103/PhysRevSTAB.14.054401

16. T.G. Blackburn, Radiation reaction in electron-beam interactions with high-intensity lasers. Rev. Mod. Plasma Phys. **4**(1), 5 (2020). https://doi.org/10.1007/s41614-020-0042-0

17. K. Poder, M. Tamburini, G. Sarri, A. Di Piazza, S. Kuschel, C.D. Baird, K. Behm, S. Bohlen, J.M. Cole, D.J. Corvan, M. Duff, E. Gerstmayr, C.H. Keitel, K. Krushelnick, S.P.D. Mangles, P. McKenna, C.D. Murphy, Z. Najmudin, C.P. Ridgers, G.M. Samarin, D.R. Symes, A.G.R. Thomas, J. Warwick, M. Zepf, Experimental signatures of the quantum nature of radiation reaction in the field of an ultraintense laser. Phys. Rev. X **8**, 031,004 (2018). https://doi.org/10.1103/PhysRevX.8.031004

18. J.M. Cole, K.T. Behm, E. Gerstmayr, T.G. Blackburn, J.C. Wood, C.D. Baird, M.J. Duff, C. Harvey, A. Ilderton, A.S. Joglekar, K. Krushelnick, S. Kuschel, M. Marklund, P. McKenna, C.D. Murphy, K. Poder, C.P. Ridgers, G.M. Samarin, G. Sarri, D.R. Symes, A.G.R. Thomas, J. Warwick, M. Zepf, Z. Najmudin, S.P.D. Mangles, Experimental evidence of radiation reaction in the collision of a high-intensity laser pulse with a laser-wakefield accelerated electron beam. Phys. Rev. X **8**, 011,020 (2018). https://doi.org/10.1103/PhysRevX.8.011020

19. A.M. Fedotov, N.B. Narozhny, G. Mourou, G. Korn, Limitations on the attainable intensity of high power lasers. Phys. Rev. Lett. **105**, 080,402 (2010). https://doi.org/10.1103/PhysRevLett.105.080402

20. A.R. Bell, J.G. Kirk, Possibility of prolific pair production with high-power lasers. Phys. Rev. Lett. **101**, 200,403 (2008). https://doi.org/10.1103/PhysRevLett.101.200403

21. J.G. Kirk, A. Bell, I. Arka, Pair production in counter-propagating laser beams. Plasma Phys. Controlled Fusion **51**(8), 085,008,008 (2009). https://doi.org/10.1088/0741-3335/51/8/085008

22. T. Grismayer, M. Vranic, J.L. Martins, R.A. Fonseca, L.O. Silva, Seeded qed cascades in counterpropagating

laser pulses. Phys. Rev. E **95**, 023,210 (2017). https://doi.org/10.1103/PhysRevE.95.023210

23. T. Grismayer, M. Vranic, J.L. Martins, R.A. Fonseca, L.O. Silva, Laser absorption via quantum electrodynamics cascades in counter propagating laser pulses. Phys. Plasmas **23**(5), 056,706 (2016). https://doi.org/10.1063/1.4950841

24. M. Vranic, T. Grismayer, R.A. Fonseca, L.O. Silva, Electron-positron cascades in multiple-laser optical traps. Plasma Phys. Controlled Fusion **59**(1), 014,040 (2016). https://doi.org/10.1088/0741-3335/59/1/014040

25. M. Tamburini, S. Meuren, Efficient high-energy photon production in the supercritical qed regime. Phys. Rev. D **104**, L091,903 (2021). https://doi.org/10.1103/PhysRevD.104.L091903

26. N.B. Narozhny, Expansion parameter of perturbation theory in intense-field quantum electrodynamics. Phys. Rev. D **21**, 1176–1183 (1980). https://doi.org/10.1103/PhysRevD.21.1176

27. V. Ritus, Radiative corrections in quantum electrodynamics with intense field and their analytical properties. Ann. Phys. **69**(2), 555–582 (1972). https://doi.org/10.1016/0003-4916(72)90191-1

28. A. Fedotov, Conjecture of perturbative qed breakdown at $\alpha\chi 2/3 \gtrsim 1$. J. Phys: Conf. Ser. **826**(1), 012,027 (2017). https://doi.org/10.1088/1742-6596/826/1/012027

29. A. Mironov, S. Meuren, A. Fedotov, Resummation of qed radiative corrections in a strong constant crossed field. Phys. Rev. D **102**(5), 053,005 (2020). https://doi.org/10.1103/physrevd.102.053005

30. R. Ekman, T. Heinzl, A. Ilderton, High-intensity scaling in uv-modified qed. Phys. Rev. D **102**(11), 116,005 (2020). https://doi.org/10.1103/physrevd.102.116005

31. X.L. Zhu, T.P. Yu, Z.M. Sheng, Y. Yin, I.C.E. Turcu, A. Pukhov, Dense gev electron-positron pairs generated by lasers in near-critical-density plasmas. Nat. Commun. **7**(1), 13,686 (2016). https://doi.org/10.1038/ncomms13686

32. P. Zhang, C.P. Ridgers, A.G.R. Thomas, The effect of nonlinear quantum electrodynamics on relativistic transparency and laser absorption in ultra-relativistic plasmas. New J. Phys. **17**(4), 043,051 (2015). https://doi.org/10.1088/1367-2630/17/4/043051

33. T.G. Blackburn, A. Ilderton, M. Marklund, C.P. Ridgers, Reaching supercritical field strengths with intense lasers. New J. Phys. **21**(5), 053,040 (2019). https://doi.org/10.1088/1367-2630/ab1e0d

34. V. Yakimenko, S. Meuren, F. Del Gaudio, C. Baumann, A. Fedotov, F. Fiuza, T. Grismayer, M.J. Hogan, A. Pukhov, L.O. Silva et al., Prospect of studying nonperturbative qed with beam-beam collisions. Phys. Rev. Lett. **122**(19), 190,404 (2019). https://doi.org/10.1103/PhysRevLett.122.190404

35. C. Baumann, E.N. Nerush, A. Pukhov, I.Y. Kostyukov, Probing non-perturbative qed with electron-laser collisions. Sci. Rep. **9**, 9407 (2019). https://doi.org/10.1038/s41598-019-45582-5

36. C. Baumann, A. Pukhov, Laser-solid interaction and its potential for probing radiative corrections in strongfield quantum electrodynamics. Plasma Phys. Controlled Fusion **61**(7), 074,010 (2019). https://doi.org/10.1088/1361-6587/ab1d2b

37. M. Filipovic, C. Baumann, A.M. Pukhov, A.S. Samsonov, I.Y. Kostyukov, Effect of transverse displacement of charged particle beams on quantum electrodynamic processes during their collision. Quantum Electron. **51**(9), 807 (2021). https://doi.org/10.1070/QEL17606

38. A. Di Piazza, T. Wistisen, M. Tamburini, U. Uggerhøj, Testing strong field qed close to the fully nonperturbative regime using aligned crystals. Phys. Rev. Lett. **124**(4), 044,801 (2020). https://doi.org/10.1103/physrevlett.124.044801

39. C.P. Ridgers, C.S. Brady, R. Duclous, J.G. Kirk, K. Bennett, T.D. Arber, A.P.L. Robinson, A.R. Bell, Dense electron-positron plasmas and ultraintense γ rays from laser-irradiated solids. Phys. Rev. Lett. **108**, 165,006 (2012). https://doi.org/10.1103/PhysRevLett.108.165006

40. A. Pukhov, Three-dimensional electromagnetic relativistic particle-in-cell code vlpl (virtual laser plasma lab). J. Plasma Phys. **61**(3), 425–433 (1999). https://doi.org/10.1017/S0022377899007515

41. R.A. Fonseca, L.O. Silva, F.S. Tsung, V.K. Decyk, W. Lu, C. Ren, W.B. Mori, S. Deng, S. Lee, T. Katsouleas, J.C. Adam, in *Computational Science – ICCS 2002*. ed. by P.M.A. Sloot, A.G. Hoekstra, C.J.K. Tan, J.J. Dongarra (Springer, Berlin Heidelberg, Berlin, Heidelberg, 2002), pp.342–351

42. J. Derouillat, A. Beck, F. Pérez, T. Vinci, M. Chiaramello, A. Grassi, M. Flé, G. Bouchard, I. Plotnikov, N. Aunai, J. Dargent, C. Riconda, M. Grech, Smilei?: A collaborative, open-source, multi-purpose particle-in-cell code for plasma simulation. Comput. Phys. Commun. **222**, 351–373 (2018). https://doi.org/10.1016/j.cpc.2017.09.024

43. A. Pukhov, Particle-in-cell codes for plasma-based particle acceleration. CERN Yellow Rep. **1**, 181 (2016). https://doi.org/10.5170/CERN-2016-001.181

44. C. Baumann, A. Pukhov, Influence of e- e+ creation on the radiative trapping in ultraintense fields of colliding laser pulses. Phys. Rev. E **94**(6), 063,204 (2016). https://doi.org/10.1103/physreve.94.063204

45. D.A. Serebryakov, E.N. Nerush, I.Y. Kostyukov, Near-surface electron acceleration during intense laser-solid interaction in the grazing incidence regime. Phys. Plasmas **24**(12), 123,115 (2017). https://doi.org/10.1063/1.5002671

46. A. Pukhov, X-dispersionless maxwell solver for plasma-based particle acceleration. J. Comput. Phys. **418**, 109,622 (2020). https://doi.org/10.1016/j.jcp.2020.109622

47. M. Tamburini, A. Di Piazza, C.H. Keitel, Laser-pulse-shape control of seeded qed cascades. Sci. Rep. **7**(1), 1–8 (2017). https://doi.org/10.1038/s41598-017-05891-z

48. A. Sampath, M. Tamburini, Towards realistic simulations of qed cascades: Non-ideal laser and electron seeding effects. Phys. Plasmas **25**(8), 083,104 (2018). https://doi.org/10.1063/1.5022640